Anthropogenic aerosol forcing and the structure of temperature trends in the southern Indian Ocean.

Wenju Cai,[1,2] Tim Cowan,[1,2] Martin Dix,[1] Leon Rotstayn,[1] Joachim Ribbe,[3] Ge Shi,[3] and Susan Wijffels[4]

Over the past decades surface warming in the southern subtropical Indian Ocean (IO) has been greater than that in other oceans. The warming penetrates to a depth of 800m, in contrast to the off-equatorial surface warming which co-exists with subsurface cooling. We examine the dynamics for this rich structure. Results from the 20th century experiments of the Intergovernmental Panel for Climate Change (IPCC) confirm that the southern subtropical IO surface-to-800m warming is greater than that in the Pacific and Atlantic Oceans. Outputs from two targeted ensemble sets of coupled model experiments, one with and one without increasing anthropogenic aerosols, show that increasing aerosols strengthen the global Conveyor, and generate a greater poleward shift and intensification of the Agulhas outflow and its retroflection; the process increases the warming rate in the subtropics, and takes heat out of the off-equatorial region generating a cooling.

1. Introduction

Historical data [*Rayner et al.*, 1996] show that since 1950 the warming trend of sea surface temperature (SST) is not uniform across the Southern Hemisphere (SH) subtropical latitudes, but is the largest in the IO (Fig. 1a). Such a pattern was not simulated by early climate models, which, under increasing CO_2, produced a fast warming rate in the Northern Hemisphere (NH), and a much slower warming rate in the SH subtropical oceans [*Cai and Whetton*, 2001]. The deficiency was attributed to some long-standing problems including a weakly stratified, overly convective modeled Southern Ocean [*Hirst and Cai*, 1994; *Toggweiler et al.*, 1989]. Implementation of an eddy-induced transport parameterization [*Gent and McWilliams*, 1990; *Duffy et al.*, 1995] onto the *Cox* [1987] isopycnal scheme improved the stratification but the model problems persisted. The inclusion of increasing aerosol forcing reduces the NH large warming rate [*Mitchell et al.*, 1995]. Here we show that aerosol forcing also improves the structure of warming trends in the SH subtropical ocean, particularly through the southern IO

[1]CSIRO Marine and Atmospheric Research, Aspendale, Victoria, Australia
[2]Wealth from Oceans National Research Flagship, CSIRO, North Ryde, New South Wales, Australia
[3]Department of Biological and Physical Sciences, University of Southern Queensland, Queensland, Australia
[4]CSIRO Marine and Atmospheric Research, Hobart, Tasmania, Australia

0094-8276/07/$5.00

sector.

Using a new compilation of historical temperature profiles, the Indian Ocean Thermal Archive (IOTA), *Alory et al.* [2007] show that the subtropical zonal-mean IO surface warming penetrates to an 800m depth (Fig. 1b), and that the IPCC models running 20th century experiments capture this surface to deep ocean warming trend. They suggested that the pattern could be explained as a 0.5° latitude poleward shift of the subtropical gyre, although no model has a fine resolution to resolve this. The off-equatorial IO surface warming in IOTA is accompanied by a subsurface cooling, which displays two centers, one 10°S at a 100m depth, and the other 17°S at 400m. The cooling at 100m might be due to a greater discharge associated with the stronger El Niños in the post-1980 period, compared with the pre-1980 period [*Shi et al.*, 2007].

There are, however, several unresolved issues. Firstly, the subtropical gyres are driven by the wind stress curl. The observed curl trend results from decreasing midlatitude westerlies and strengthening high-latitude westerlies as a consequence of a poleward shift of the westerly jet incorporated into the upward trend in the Southern Annular Mode (SAM) [*Saenko et al.*, 2005; *Cai*, 2006]. The SAM trend over the past decades is related to the Antarctic ozone depletion [*Thompson and Solomon*, 2002; *Gillett and Thompson*, 2003; *Cai and Cowan*, 2007]. Yet *Alory et al.*, [2007] found that the IPCC models that include an ozone depletion forcing do not show a greater subtropical IO warming than those without. Thus differences in other forcing must be considered. Secondly, the off-equatorial cooling 17°S at 400m (Fig. 1b) has not been fully explained. Finally, although observations show a greater subtropical surface IO warming, the warming rate at depth relative to that in other oceans is not clear. If surface warming is an indication of deep warming, then Fig. 1a means that the subtropical IO deep warming is greater than that in other oceans. This seems to be borne out by the IPCC models. We will examine the dynamics of this feature.

Although the majority of the IPCC experiments include an aerosol forcing, there is no outputs from the same model that singles out the impact of aerosol forcing. To this end, we analyze outputs from two newly available ensemble sets, one with aerosols fixed at the preindustrial level and another that incorporates increasing aerosols through an interactive aerosol scheme [*Rotstayn et al.*, 2007].

2. Data and model and experiments

The atmospheric model, used in this study, is a low-resolution, flux adjusted (spectral R21) version of the CSIRO atmospheric general circulation model. The R21 model has 18 hybrid vertical levels and a horizontal resolution of approximately 5.6° in longitude and 3.2° in latitude. The oceanic component is based on the Cox-Bryan code [*Cox*, 1984], and has the same horizontal resolution as the atmospheric model, with 21 vertical levels. The model has a comprehensive aerosol scheme in the simulations for the period 1871 to 2000, with and without the effects of increasing anthropogenic aerosols. We focus on the period since 1951. The aerosol species treated interactively are sulfate, particulate organic matter (POM), black carbon (BC), mineral dust and sea salt. Historical emission inventories are used for sulfur, POM and BC derived from the burning of fossil fuels and biomass. Other

forcings included are those due to changes in long-lived greenhouse gases, ozone, volcanic aerosol and solar variations. An eight-run ensemble with all of these forcings (ALL ensemble) and a further eight runs with all forcings except those related to anthropogenic aerosols (AXA ensemble) were performed. The AXA ensemble only differs from that of the ALL ensemble in that the anthropogenic emissions of sulfur, POM and BC are fixed at their 1870 levels. We also deploy a multi-century control climate to assess the significance of the difference between ALL and AXA, as described in *Cai et al.*, [2006].

3. Model evidence of greater subtropical Indian Ocean warming

The ensemble mean of the IPCC models used in the *Alory et al.* [2007] study reproduces a stronger surface warming in the subtropical IO than that in other oceans (Fig. 1c) and the latitude-depth structure (Fig. 1d) with warming penetrating to 800m. The subsurface cooling 10°S at 100m does not show up because most models do not produce a greater ENSO discharge after 1980. The contrast between the IO and the Pacific-Atlantic sector is also seen in depth-averaged warming (Fig. 2). The ensemble IO warming (black curve) is greater than that in the IOTA (blue line), and the Pacific and Atlantic Oceans (orange curve), but the feature of warming maximum located in the latitude band 40°S-50°S is well simulated. At the latitude of largest warming, 43°S, the standard deviation of the spread is 0.29°C century^{-1}, far smaller than the ensemble trend at this latitude.

These contrasts between the IO and the Pacific-Atlantic sector are produced in both ALL (Figs. 3a-3c) and AXA (Figs. 3d-3f), but important differences exist between the two sets. Firstly, except in the subtropical IO, where the warming is more pronounced in ALL, warming trends are generally smaller in ALL. This is because the increasing aerosols cool both the NH and SH oceans through a pan-oceanic adjustment with a strengthening cross-hemispheric transport from the SH oceans to the NH oceans [*Cai et al.*, 2006], particularly to the North Atlantic. The process mitigates an increasing CO_2-induced slowdown of the North Atlantic Deep Water Formation (NADWF). Secondly, the contrast between the subtropical IO deep warming and that in other oceans is sharper in ALL. Finally, the off-equatorial subsurface cooling 17°S at 400m is only produced in ALL; as will be discussed later, in ALL, the strengthening of the cross-hemispheric heat transport to the NH oceans is not derived uniformly from the SH oceans, but mostly along the Conveyor associated with the NADWF, including the subtropical IO (see section 4).

4. Dynamics for a stronger subtropical IO warming

The fundamental forcing of the southern subtropical IO warming is a poleward shift of the southern subtropical gyre. There are two reasons for a stronger warming in the IO than in the other oceans. Firstly, the climatological wind stress curl over the subtropical IO is far greater than that over the other oceans [lower panels of Fig. 2, *Cai*, 2006]. This is determined, in turn, by a sharper meridional SST gradient in the subtropical IO, because north of the subtropical latitudes there is significant heat input by the Indonesian Throughflow (ITF). The stronger meridional SST gradient supports

stronger meridional gradients of zonal wind, and hence stronger wind stress curls. The integrated curl from the eastern to western boundary is greater in the IO, hence the wind-driven subtropical gyre is stronger than in the other oceans. Secondly, the subtropical IO gyre has a significant buoyancy-driven component, as it is a part of the global Conveyor pathway, carrying an additional 10 Sv [*Gordon*, 1986] in the Agulhas outflow, some of which eventually compensate the NADWF. These factors determine that the climatological IO subtropical gyre is far larger than in other oceans [*Gordon*, 1985]. Thus, for an equal extent of a poleward shift, a greater warming will be generated in the IO than in other oceans. This explains the greater warming in the subtropical IO than in the subtropical Pacific and Atlantic in AXA (see Fig. 3e and Fig. 3f). However, in AXA the contrast between the IO warming rate and that in other oceans is weak (Figs. 3a and 3d).

The forcing of increasing aerosols improves the trend pattern of the IO. Firstly, in the off-equatorial IO, the cooling 17°S at 400m depth is only present in ALL. As discussed in *Cai et al.* [2006] and *Delworth and Dixon* [2006], aerosol-induced cooling leads to a more stable NADWF. In fact, in ALL there is a slight increase in the NADWF, whereas in AXA, the NADWF weakens slightly. The difference in the NADWF (ALL minus AXA) is about 1.3 Sv (10%). The difference in the NADWF, the associated cross-equatorial heat transport, and the oceanic heat content, has shown to be statistically significant at a 99% confidence level [*Cai et al.*, 2006]. The upper branch of the Conveyor (ocean currents averaged over upper-800m) strengthens in ALL with increasing ITF and flows toward the North Atlantic (Fig. 4a), as opposed to a weaker global Conveyor and ITF in AXA (Fig. 4b). In ALL, the heat for supporting the stronger NADWF is derived along the Conveyor pathway of the SH oceans, including the off-equatorial IO, leading to the subsurface cooling 17°S at 400m depth (Fig. 4a, contour; Fig. 3b). Figure 4a suggests that such a subsurface cooling takes place in the off-equatorial Pacific and Atlantic Oceans as well. By contrast, in AXA there is an accumulation of heat in the off-equatorial region (Fig. 4b). Secondly, increasing aerosols sharpen the contrast between the SH subtropical IO warming and that in the other oceans (Fig. 4a, contour). This is because the poleward shift and intensification of the subtropical IO gyre, and hence the midlatitude IO warming, is far greater in ALL than in AXA, as further illustrated in Figs. 5a and 5c: in ALL the streamfunction trend has a maximum of 4.9 Sv at 45°S, compared with a value less than 1 Sv at 42°S in AXA.

That the origin of the large warming in ALL lies in the ocean is supported by a heat loss trend in the midlatitude IO where the warming is largest (figure not shown). The poleward intensification of the subtropical IO gyre is so powerful and generates such a large warming that it has to lose heat to the atmosphere. It turns out that a positive air-sea feedback ensues: the stronger Agulhas outflow and retroflection due to the stronger NADWF initially shift the location of the maximum SST gradient and maximum atmospheric baroclinicity polewards, reducing storm activities and westerlies to the north, and taking less heat out of the ocean there; to the south storms and westerlies increase, cooling the ocean [*Inatsu and Hoskin*, 2004]. This leads to a greater meridional SST gradient, which generates stronger westerlies polewards and increasing wind stress curl, leading to stronger wind and curl trends in ALL (Figs. 5b and 5d). The stronger curl

trend in turn supports the strong poleward shift and intensification of the subtropical IO gyre [*Cai et al.*, 2007].

5. Conclusions

Over the past decades, the surface warming trend in the southern subtropical IO has been greater than that in other southern subtropical oceans. A new compilation of the IO Temperature Archive indicates that the subtropical IO surface warming penetrates to an 800m depth, in contrast to the off-equatorial region, where surface warming is accompanied by subsurface cooling. Here we show that the southern subtropical deep-warming in the IO is also greater than that in the Pacific and Atlantic Oceans. Although a poleward shift of the southern subtropical gyre occurs with or without forcing of increasing aerosols, the IO trend pattern is better simulated with increasing aerosols. This is because increasing aerosols mitigate the global Conveyor from an increasing CO_2-induced slow-down, generating a greater cross-hemisphere heat transport. The heat is derived along the pathway of the Conveyor. In association a stronger Agulhas outflow and retroflection are generated. The stronger outflow leads to a stronger warming rate in the subtropical latitudes and takes heat out the off-equatorial IO, generating the off-equatorial subsurface cooling and the large subtropical warming. We note that the cooling effect of increasing aerosols in our model may be over-estimated as it leads to generally a too small a warming rate in the SH oceans. However, it improves the spatial structure of warming trends in the southern IO, particularly the generation of off-equatorial subsurface cooling, concentrated warming in the subtropical IO, and its contrast with the subtropical Pacific and Atlantic Oceans.

Acknowledgments. This work is supported by the Australian Greenhouse Office. We thank members of the CSIRO Climate Model and Applications Team for developing the model. We thank G. Alory for reviewing the paper before submission, and two anonymous reviewers for their helpful comments.

References

Alory, G., S. Wijffels, and G. Meyers (2007), Observed temperature trends in the Indian Ocean over 1960-1999 and associated mechanisms, *Geophys. Res. Lett.*, *34*, L02606, doi:10.1029/2006GL028044.

Cai W., and P. H. Whetton (2001), A time-varying greenhouse warming pattern and the tropical-extratropical circulation linkage in the Pacific Ocean, *J. Clim*, *14*, 3337–3355.

Cai, W. J. (2006), Antarctic ozone depletion causes an intensification of the southern ocean super-gyre circulation, *Geophys Res. Lett.*, *33* (3): L03712, 10.1029/2005GL024911.

Cai, W., and T. Cowan (2007a), Trends in Southern Hemisphere Circulation in IPCC AR4 Models over 1950-99: Ozone Depletion versus Greenhouse Forcing, *J. Clim*, *20 (4)* 681–693.

Cai, W., and T. Cowan (2007), An air-sea positive feedback in the generation of the SAM trend. *J. Geophys. Res.*, submitted.

Cai, W., D. Bi, J. Church, T. Cowan, M. Dix, and L. Rotstayn (2006), Pan-oceanic response to increasing anthropogenic aerosols: Impacts on the Southern Hemisphere oceanic circulation, *Geophys. Res. Lett.*, *33*, L21707, doi:10.1029/2006GL027513.

Cox, M. D. (1984), A primitive equation, 3-dimensional model of the ocean. GFDL Ocean Group Tech. Rep. No. 1, 143 pp.

Cox, M. D. (1987), Iospycnal diffusion in a z-coordinate ocean model, *Ocean Modelling*, *74*, 1–5.

Delworth, T. L., and K. W. Dixon (2006), Have anthropogenic aerosols delayed a greenhouse gas-induced weakening of the North Atlantic thermohaline circulation? *Geophys. Res. Lett.*, *33*, L02606, doi:10.1029/2005GL024980.

Duffy, P. B. and P. Eltgroth, A. J. Bourgeois, and K. Caldeira (1995), Improved representation of vertical profiles of temperature and bomb radiocarbon in GFDF ocean general circulation, *Geophys. Res. Lett.*, *22*, 1065–1068.

Gent, P. R. and J. C. McWilliams (1990), Isopycnal mixing in ocean circulation models. *J. Phys. Oceanogr.*, *20*, 150–155.

Gillett, N. P., and D. W. J. Thompson (2003), Simulation of recent Southern Hemisphere climate change, *Science*, *302*, 273–275.

Gordon, A. L. (1985), Indian-Atlantic transfer of thermocline water at the Agulhas Retroflection, *Science*, *227*, 1030–1033.

Gordon, A. L. (1986), Interocean exchange of thermocline water, *J. Geophys. Res.*, *91*, 5037–5046.

Hirst, A. C., W. J. Cai (1994), Sensitivity of a World ocean GCM to subsurface parameterization, *J. Phys. Oceanogr.*, *24*, 1256–1279.

Inatsu, M., and B. J. Hoskins (2004), The zonal asymmetry of the Southern Hemisphere winter storm-track, *J. Climate*, *17*, 4882–4892.

Mitchell, J. F. B., T. C. Johns, J. M. Gregory, and S. F. B. Tett (1995), Climate response to increasing levels of greenhouse gases and sulphate aerosols, *Nature*, *376*, 501–504.

Rayner, N. A., E. B. Horton, D. E. Parker, C. K. Folland, and R. B. Hackett (1996), Version 2.2 of the Global sea-Ice and Sea Surface Temperature dataset, 1903-1994. Climate Research Tech. Note CRTN74, Hadley Centre, Met Office, Bracknell, Berkshire, United Kingdom, 25 pp.

Rotstayn, L. D., W. Cai, M. R. Dix, G. D. Farquhar, Y. Feng, P. Ginoux, M. Herzog, A. Ito, J. E. Penner, M. L. Roderick, and M. Wang (2007), Have Australian rainfall and cloudiness inceased due to the remote effects of anthropogenic aerosols? *J. Geophys. Res.*, 112, D09202, doi:10.1029/2006JD007712

Saenko, O. A., J. C. Fyfe, and M. H. England (2005), On the response of the oceanic wind-driven circulation to atmospheric CO2 increase, *Clim. Dyn.*, *25*, 415–426, doi: 10.1007/s00382-005-0032-5.

Shi, G., J. Ribbe, W. Cai, and T. Cowan (2007), Multidecadal variability in the transmission of ENSO signals to the Indian Ocean in SODA-POP and in a coupled climate model, *Geophys. Res. Lett.*, 34, L09706, doi:10.1029/2007GL029528.

Thompson, D. W. J., and S. Solomon (2002), Interpretation of recent Southern Hemisphere climate change, *Science*, *296*, 895–899.

Toggweiler, J. R., K. Dixon, and K. Bryan (1989), Simulation of radiocarbon in coarse-resolution World Ocean model. Part I: steady state prebomb distributions, *J. Geophys. Res.*, *94*, 8217–8242.

W. Cai, CSIRO Marine and Atmospheric Research, PMB 1, Aspendale, Victoria 3195, Australia. (wenju.cai@csiro.au)

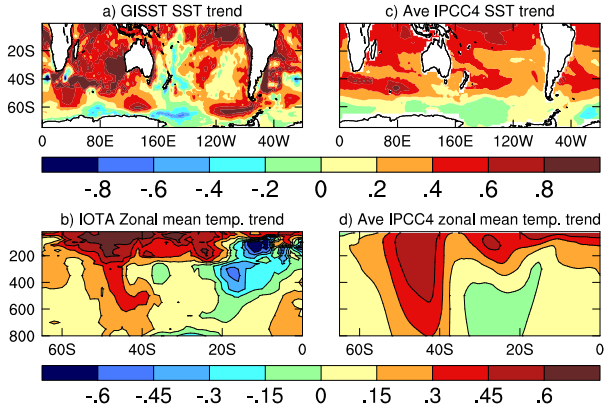

Figure 1. Trends over 1951-2000 of observed global SST (a), and zonal mean temperature of the upper 800 m over the Indian Ocean sector from IOTA (b); c) and d), the same as a) and b) but averaged over the IPCC models used in the *Alory et al.* [2007] study. Units are in °C per 50 years.

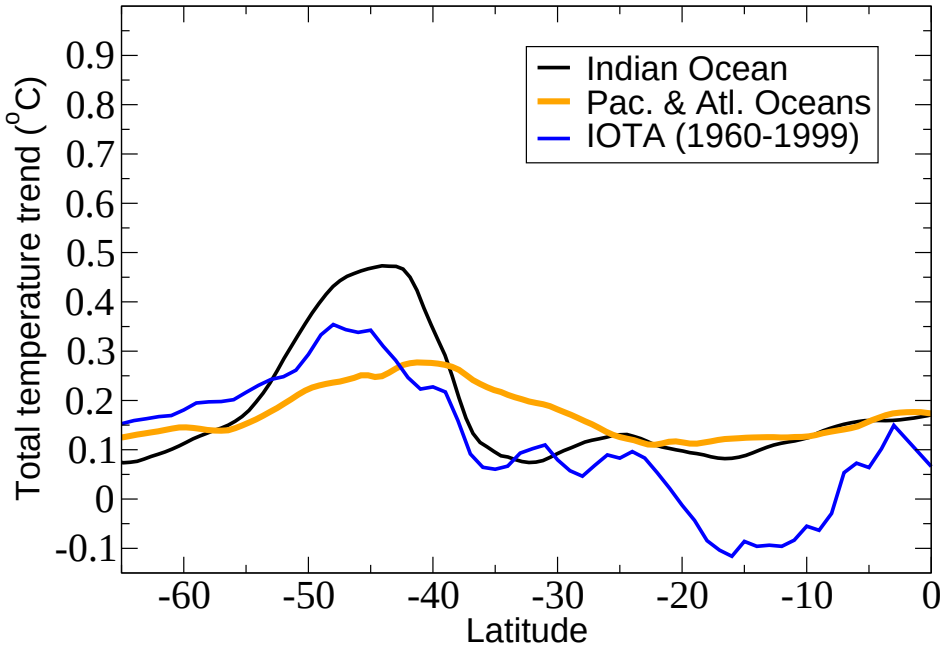

Figure 2. Upper 800m average of zonal-mean temperature trends for the 1951-2000 period for the Indian Ocean sector (black line), and for the Pacific-Atlantic sectors combined (orange line) from the IPCC models used in the *Alory et al.* [2007] study. Comparisons to observations are from the Indian Ocean Temperature Archive (IOTA) for the 1960-1999 period (blue line). Units are in °C per 50 years.

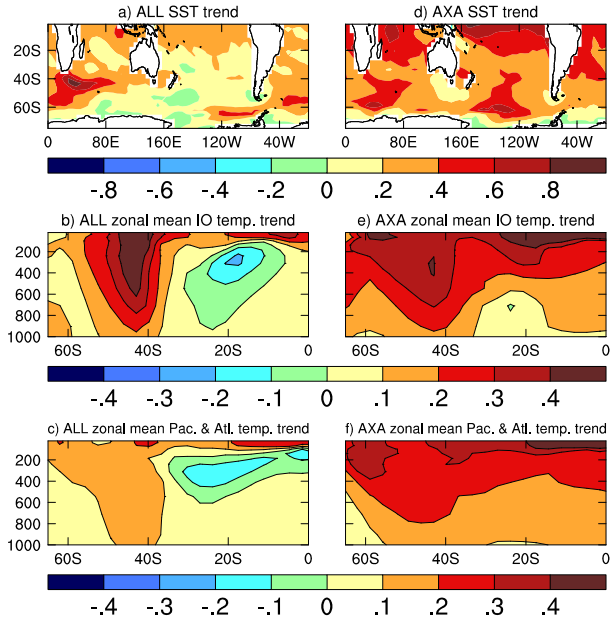

Figure 3. Trends over 1951-2000 of global SST (a) and zonal mean temperature of the upper 800 m over the Indian Ocean sector (b), and over the Pacific-Atlantic sectors combined (c) in the ALL ensemble, i.e., with increasing aerosols. Panels (d) -(f), the same as (a) - (c) but for the AXA ensemble, i.e., without increasing aerosols. Units are in °C per 50 years.

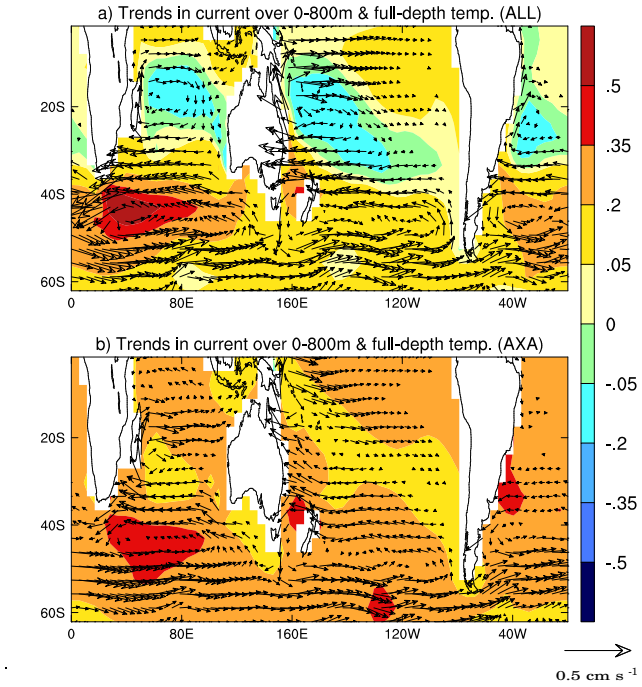

Figure 4. Trends of upper-800m oceanic heat content, in terms of vertically averaged temperature, superimposed on vertically averaged oceanic currents (cm s^{-1} per 50 years) over the same depth range for the ALL (upper panel) and for the AXA (lower panel) ensemble. Units are in °C per 50 years.

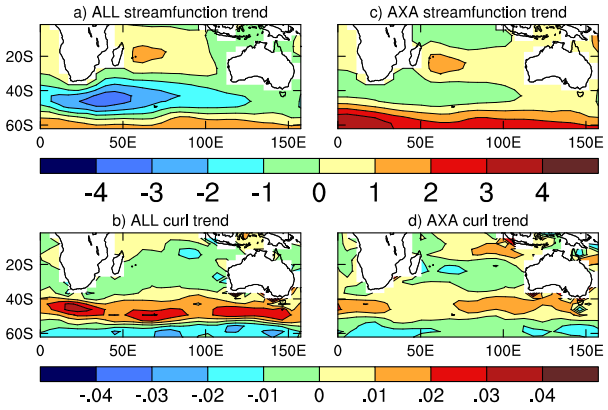

Figure 5. Trends of streamfunction (left column, Sv per 50 years), wind stress curl (second, 10^{-6} N m^{-3} per 50 years) for ALL (upper panel) and AXA (lower panel).